SURE 静岡大学学術リポジトリ
Shizuoka University REpository

Designed abscisic acid analogs as antagonists of PYL-PP2C receptor interactions

メタデータ	言語: English 出版者: 公開日: 2014-11-07 キーワード (Ja): キーワード (En): 作成者: Takeuchi, Jun, Okamoto, Masanori, Akiyama, Tomonori, Muto, Takuya, Yajima, Shunsuke, Sue, Masayuki, Seo, Mitsunori, Kanno, Yuri, Kamo, Tsunashi, Endo, Akira, Nambara, Eiji, Hirai, Nobuhiro, Ohnishi, Toshiyuki, Cutler, Sean R, Todoroki, Yasushi メールアドレス: 所属:
URL	http://hdl.handle.net/10297/7954

Designed abscisic acid analogs as antagonists of PYL-PP2C receptor interactions

Jun Takeuchi[1,13], Masanori Okamoto[2,3,13], Tomonori Akiyama[4], Takuya Muto[5], Shunsuke Yajima[4], Masayuki Sue[6], Mitsunori Seo[7], Yuri Kanno[7], Tsunashi Kamo[8], Akira Endo[9,12], Eiji Nambara[9], Nobuhiro Hirai[10], Toshiyuki Ohnishi[5,11], Sean R Cutler[3] &Yasushi Todoroki[1,5,11]*

[1]Graduate School of Science and Technology, Shizuoka University, Shizuoka , Japan. [2]Arid Land Research Center, Tottori University, Tottori , Japan. [3]Department of Botany and Plant Sciences and Center for Plant Cell Biology, University of California–Riverside, Riverside, California, USA. [4]Department of Bioscience, Tokyo University of Agriculture, Tokyo, Japan. [5]Graduate School of Agriculture, Shizuoka University, Shizuoka, Japan. [6]Department of Applied Biology and Chemistry, Tokyo University of Agriculture, Tokyo, Japan. [7]RIKEN Center for Sustainable Resource Science, Kanagawa, Japan. [8]National Institute for Agro-Environmental Sciences, Ibaraki, Japan. [9]Department of Cell and Systems Biology, University of Toronto, Toronto, Ontario, Canada. [10]Graduate School of Agriculture, Kyoto University, Kyoto, Japan. [11]Research Institute of Green Science and Technology, Shizuoka University, Shizuoka , Japan. [12]Present address: Crop Breeding Research Division, National Agricultural Research Organization for Hokkaido Region, Hokkaido, Japan. [13]These authors contributed equally to this work.

*e-mail: aytodor@ipc.shizuoka.ac.jp

The plant stress hormone abscisic acid (ABA) is critical for several abiotic stress responses. ABA signaling is normally repressed by group-A protein phosphatases 2C (PP2Cs), but stress-induced ABA binds *Arabidopsis* PYR/PYL/RCAR (PYL) receptors, which then bind and inhibit PP2Cs. X-ray structures of several receptor–ABA complexes revealed a tunnel above ABA's 3′ ring CH that opens at the PP2C binding interface. Here, ABA analogs with sufficiently long 3′ alkyl chains were predicted to traverse this tunnel and block PYL-PP2C interactions. To test this, a series of 3′-alkylsulfanyl ABAs were synthesized with different alkyl chain lengths. Physiological, biochemical and structural

analyses revealed that a six-carbon alkyl substitution produced a potent ABA antagonist that was sufficiently active to block multiple stress-induced ABA responses *in vivo*. This study provides a new approach for the design of ABA analogs, and the results validated structure-based design for this target class.

Several plant hormones function as natural modulators of protein-protein interactions (PPIs) and ultimately modulate the affinity of hormone receptors for their protein binding partners[1,2]. Indole-3-acetic acid, jasmonate-isoleucine conjugate and brassinosteroids act as molecular glues that stabilize PPIs without causing major conformational changes of their receptor proteins, whereas ABA and gibberellin (GA) are allosteric ligands that cause conformational changes in their receptors that are required for PPIs[1,3,4]. Although PPIs have recently emerged as attractive drug targets, the rational design of small molecules that act as positive or negative PPI modulators remains challenging, in part because of the difficulty in creating tight interactions with the relatively flat, large and featureless interfaces typical of PPIs[5]. In the case of plant hormones, such as ABA and GA, the challenge is different because these hormones bind within a cavity and induce conformational changes as opposed to binding between two flat surfaces. Given this feature, it may be easier to manipulate these types of PPIs. However, with the exception of a GA receptor inhibitor that was discovered using chemical screening [6], the successful, rational design of PPI inhibitors has been limited to rigid receptors, which do not induce conformational changes[7–9]. Alternative design strategies are thus required for creating allosteric modulators, and such efforts benefit from known structural details of ligand-induced conformational changes; the ABA receptor system currently provides this data better than any other plant system[10–20].

ABA has critical roles in many physiological processes, such as seed dormancy, stomatal closure and adaptive responses to abiotic stress[21,22]. The physiological effects of ABA are controlled by signal transduction through the PYL ABA receptors, which are members of

the START superfamily of ligand-binding proteins[23,24]. *Arabidopsis* PYLs are classified into two distinct subclasses: dimeric receptors (PYR1 and PYL1–3) and monomeric receptors (PYL4–12)[10,11]. Dimeric receptors, which are inactive in the absence of ABA, dissociate into monomers in response to a conformational change induced by ABA binding, which triggers the closure of a mobile gating loop. This gate is open in the apoenzyme state but closes to create an interaction surface that enables binding to the active site of group-A PP2Cs, including HAB1, ABI1 and ABI2 (refs. 13, 16, 19–25). ABA-bound PYLs interact with and inhibit PP2Cs, which directly inactivate SNF1-related protein kinases (SnRK2s) in the absence of ABA to allow the activation of SnRK2s via autophosphorylation[25–27]. Activated SnRK2s phosphorylate transcription factors and S-type anion channels to elicit ABA actions[26,28–31]. Thus, in this system, the activity of the key regulatory SnRK2 kinases is controlled by ABA-mediated inhibition of PP2C activity. In contrast to dimeric receptors, monomeric receptors are in equilibrium between the gate-opened and gate-closed conformers in the absence of ABA[10,11]. Thus, monomeric receptors can inhibit PP2C activity in the absence of ABA[10,11,24,32], although at a much lower level than that observed in the presence of ABA[10]. Previous studies have indicated that both dimeric and monomeric receptors are involved in plant ABA responses[33,34]; however, the physiological importance of ABA-independent PP2C inhibition by monomeric receptors remains unresolved. It has additionally been demonstrated that selective chemical activation of the dimeric receptors elicits a nearly full ABA response, which points to dimeric receptors as key factors in ABA signaling[35].

Although numerous ABA receptor agonists have been described[14,36], little work has been done regarding antagonists. Given the role of ABA in numerous stress responses across virtually all land plants, a tool for inhibiting ABA signaling would be extremely valuable for dissecting ABA's myriad roles, particularly in new systems lacking genetic resources. Additionally, ABA-receptor antagonists are of potential agrichemical value because, in a

number of crop species, the ability to control seed germination rates, which are affected by ABA, is important. Moreover, ABA inactivation in pollen has been associated with improved grain yield under stress in some cereal varieties[37], which highlights one potential use for ABA antagonists. It has been previously shown that the sulfonamide pyrabactin (PyrA) is a selective agonist of PYR1 and PYL1 and a weak antagonist of PYL2, but its stronger agonist activity dominates its effects, and it is an ineffective antagonist *in vivo*. Thus, there is a real need to create antagonists for use in multiple contexts.

As the actions of PYL proteins are connected to ligand-mediated gate closure, an effective antagonist might stabilize gate-opened conformers; that is, it might function as an inverse agonist. Alternatively, antagonists might enable gate closure but block PP2C binding and inhibition.

Here, we describe simple modifications of ABA that convert it into an antagonist capable of blocking PYL-PP2C binding. Structure-guided design was used to create ABA receptor antagonists, 3′-alkylsulfanyl-ABAs, and their effects on ABA signaling were examined. 3′-Hexylsulfanyl-ABA (which contains a six-carbon alkyl substitution, henceforth referred to as AS6; **7**) bound PYLs with an affinity comparable to that of ABA and inhibited ABA-induced PYL-PP2C interactions through direct steric hindrance by its *S*-hexyl chain and consequently blocked plant ABA responses. Thus, we demonstrate that AS6 acts as a functional ABA receptor antagonist both *in vitro* and *in vivo*.

RESULTS

Design and synthesis

The 2', 3' and 4' positions of ABA's ring were found to participate in gate closure via hydrophobic contacts to the gate loop, and, furthermore, multiple PYL-ABA X-ray structures revealed that gate closure was accompanied by the formation of two small solvent-exposed

tunnels adjacent to ABA's 3′-CH and 4'-C=O (**Supplementary Results**, **Supplementary Fig. 1a**,**b**). The entrance to these tunnels (referred to as 3′- and 4'-tunnels) lay on the interface that normally contacted PP2C. The 3′ tunnel was a relatively simple cleft formed by five highly conserved hydrophobic residues (in PYR1: Phe61, Leu87, Pro88, Phe159 and Val163; **Supplementary Fig. 1c**–**f**). Because some 3′-modified analogs of ABA retained activity (**Supplementary Table 1**)[36,38], it was reasoned that the 3′ tunnel might have accepted alkyl substituents at the 3′ position that could then form hydrophobic contacts with the tunnel. One might have expected such derivatives to potentially stabilize the gate-closed conformer, interfere with gate closure or, in the case of longer chains, protrude through the tunnel and prevent PP2C binding. Thus, alterations of chain length could conceivably have resulted in both agonists and antagonists, making this an interesting site for ABA modifications.

On the basis of the above considerations, 3′-alkylsulfanyl ABAs (**3**-**13**) were designed by nucleophilic addition of alkyl thiolate to the 2′,3′-epoxides **2**, prepared from ABA (**1**; **Fig. 1a**). For simplicity, these are called the AS*n* compound series, where *n* denotes the alkyl chain length. Before preparing these compounds, a model of a PYR1–AS6 complex was constructed on the basis of crystal structures of PYR1–ABA complexes[17,18]. This model suggested that a hexyl chain was of sufficient length to protrude through the PYR1 surface (**Supplementary Fig. 3a**) and occupy a position normally occupied by the highly conserved PP2C residue Val393 (HAB1 numbering; **Supplementary Fig. 3b**). Therefore, AS6 was predicted to bind PYR1's ligand-binding pocket and disrupt PP2C binding. These analyses also suggested that compounds with $n < 4$ might stabilize gate closure and act as agonists. The validity of these predictions was established by the synthesis and characterization of 11 AS*n* compounds ($n = 2$–12; **Fig. 1a**).

Physiological effects of AS*n* on plants

As these compounds' activities *in vivo* were of paramount importance, the effects of AS*n* compounds were examined first using seed germination assays, which rely on ABA's inhibitory effect on germination to distinguish between antagonist or agonist activities. Here, agonists inhibit seed germination, and antagonists relieve this inhibition when coapplied with ABA. These experiments showed that AS2 and AS3 inhibited *Arabidopsis* seed germination and early seedling growth and that the potency of AS2 was greater than that of ABA (**Fig. 1b** and **Supplementary Fig. 4**). *In vivo*, ABA is inactivated by cytochrome P450–mediated hydroxylation by CYP707A enzymes[39,40]. AS2 inhibited CYP707A with a K_i value of 56 μM, which was approximately tenfold higher than the K_m for ABA (4.8 μM; **Supplementary Table 2**). The slightly greater bioactivity of AS2 might therefore have been a consequence of decreased metabolic inactivation by CYP707A enzymes[41]. AS4 was a weaker agonist than AS2 and AS3, and molecules with $n > 4$ did not inhibit germination. AS2–AS4 enhanced and AS5–AS12 suppressed ABA's effect on germination and early seedling growth in coapplications with ABA (**Fig. 1c** and **Supplementary Figs. 4** and **5**). The suppression of ABA effects by the latter compounds suggested that they were receptor antagonists.

A similar trend was observed in studies with *Lactuca sativa* (lettuce), which showed that AS*n* compound effects were not restricted to *Arabidopsis* (**Supplementary Figs. 6** and **7**). The effects of AS2, AS4 and AS6 were also tested on *Raphanus sativus* (radish) seedling drought tolerance. Treatments with AS2 reduced water loss and enhanced drought tolerance (**Supplementary Table 3** and **Supplementary Fig. 8**), as expected of an agonist. Conversely, AS6-treated seedlings lost water more rapidly, showed reduced leaf temperatures (owing to increased evaporative cooling) and wilted more quickly than mock-treated controls (**Supplementary Fig. 9**), consistent with expected antagonist effects. Thus, the AS*n* compound

series contained both agonist and antagonist activities with good bioavailabilities and activities beyond the model plant.

The molecular bases of AS2, AS4 and AS6 actions *in vivo* were further characterized in *Arabidopsis*. AS2 was found to induce expression of ABA-responsive genes and the β-glucuronidase (GUS) gene on an ABA-responsive, transcriptional, reporter line with slightly stronger activity than ABA, which was consistent with the seed germination data (**Fig. 2a**,**b**). With AS4, clear expression of ABA-responsive genes was not observed by qRT-PCR, but weak reporter gene activation was detected in root tissues (**Fig. 2a**,**b**). As expected, AS6 was not able to induce obvious ABA responses, as measured by both qRT-PCR gene expression and reporter line assays (**Fig. 2a**,**b**). AS2 enhanced expression of ABA-inducible genes, whereas AS4 and AS6 lessened their expression in cotreatment with ABA (**Fig. 2c**,**d**). This antagonist effect was stronger for AS6 than AS4, the latter only partially decreasing expression of these genes. Notably, AS6 also repressed expression of stress-induced ABA-responsive genes in response to treatment with mannitol, which induced ABA synthesis by mimicking the water loss caused by drought (**Supplementary Fig. 10**). These physiological data suggested that AS2 and AS6 functioned as a PYL agonist and antagonist, respectively, whereas AS4 exhibited an intermediate effect, consistent with predictions based on the present PYR1–AS6 model (**Supplementary Fig. 3**).

PyrA is a synthetic PYL agonist but not an ABA analog and inhibits seed germination primarily by activating PYR1 (ref. 24). Additionally, it has weak antagonist activity in assays with PYL2 *in vitro*, which perhaps explains its inability to trigger a strong ABA response in adult plant tissues. Given this, the two compounds were compared, and, consistent with previous reports[24,35], PyrA was observed not to induce strong ABA responses in vegetative tissues. More notably, PyrA, unlike AS6, did not block induction of ABA-inducible genes by either exogenous ABA treatment or endogenous stimulation by mannitol treatment (**Fig. 2c**,**d**

and **Supplementary Fig. 10**). Therefore, the previously reported PYL2-selective antagonist activity of PyrA[14] seemed not to be physiologically relevant, and, notably, the reported activity required a high molar excess of PyrA relative to ABA *in vitro* to be observed.

Biochemical characterization of AS*n*

The 3′ tunnel is enclosed by highly conserved residues, and therefore it was expected that AS*n* compounds might have broad-spectrum activity across the receptor family. Thus, the effects of AS*n*s on 11 of the 13 *Arabidopsis* receptors were examined using phosphatase assays (PYL7 and PYL12 have remained recalcitrant to expression as active proteins in our hands). In these assays, receptor activation was monitored by PP2C activity inhibition, and effective agonists exhibited near-complete PP2C activity inhibition at saturating concentrations, whereas partial agonists failed to completely inhibit PP2C activity. AS2 activated dimeric receptors (PYR1 and PYL1–3) with potencies comparable to that of ABA (**Fig. 3a**) and showed incomplete activation of the monomeric receptors PYL4, PYL5 and PYL11; thus, AS2 was not a broad-spectrum agonist. The recently reported agonist quinabactin also primarily activates dimeric receptors, and the AS2 effects observed here provided independent evidence for the sufficiency of dimeric receptors to activate ABA responses[34]. AS4 displayed incomplete activation of dimeric receptors compared to ABA, and AS6 was also able to partially cause activation. Although AS6 bound to PYLs with affinity comparable to ABA, as described below, its effects included less than 50% PP2C inhibition, which suggested that AS6 acted as a weak partial agonist.

The antagonist activities of these compounds *in vitro* were characterized by examining their ability to reverse ABA-mediated PP2C inhibition. These experiments showed that AS4 and AS6 antagonized ABA-dependent PP2C inhibition for all of the receptors tested, indicating broad-spectrum antagonist activity (**Fig. 3** and **Supplementary Fig. 11**). AS6's effects were greater than those of AS4, but neither enabled full recovery of PP2C activity, even when

present at a 20-fold excess over ABA. This might be explained by the intrinsic partial-agonist activity of AS6 and, thus, in the presence of ABA, AS6 only enabled PP2C activity recovery to ~50% of the inhibition observed in the presence of AS6 alone.

The mechanism of AS6 antagonist activity was further characterized by pulldown assays *in vitro* using recombinant PYLs in combination with HAB1. In cotreatment experiments, AS6 blocked ABA-induced PYL-PP2C interactions in a dose-dependent manner (**Supplementary Fig. 11**), as expected for an antagonist. AS6 did not block ABA-independent interactions of PYL6, PYL8 and PYL10 with HAB1 but did reduce their ABA-dependent interactions (**Supplementary Fig. 11**). These biochemical data showed that AS6 acted as an antagonist by blocking ABA-induced PYL-PP2C interactions.

Thermodynamic and structural analysis of PYL–AS6 complexes

Isothermal titration calorimetry was next used to characterize AS6 binding with monomeric receptors, which were selected over dimeric receptors because they display simple ligand association and dissociation and lack a dimer dissociation step. These analyses revealed apparent dissociation constants (K_d) of 0.48 ± 0.10 μM (s.e.m.) and 1.28 ± 0.72 μM (PYL5 and PYL10, respectively) with negative enthalpies, indicating an exothermic binding process (**Supplementary Fig. 12** and **Supplementary Table 4**). These values were comparable to those of ABA (0.88 ± 0.11 μM and 0.78 ± 0.12 μM for PYL5 and PYL10, respectively. In comparison to ABA, AS6 binding to PYL5 was associated with larger negative enthalpy and entropy. In contrast, this was not the case for AS6-PYL10 interactions, which suggested that there might have been subtle mechanistic differences in the AS6 gate-closing dynamics for different receptors.

The molecular mechanism of AS6 activity was then clarified by determining the crystal structure of recombinant PYR1 bound to AS6 at 2.3-Å resolution, using molecular replacement

and starting from published PYR1–ABA coordinates (Protein Data Bank (PDB) code 3K90; refinement and structure statistics are summarized in **Supplementary Table 5**). The PYR1–AS6 complex was found to resemble very closely that of the PYR1–ABA complex (**Fig. 4a**), and AS6's ABA-skeleton resided in almost the same position normally occupied by ABA (**Fig. 4b**). Consistent with the present model-based predictions, the gate loop adopted a closed conformation, and the 3′ tunnel accommodated the AS6 *S*-hexyl chain, which also protruded out onto PYR1's PP2C-interaction surface (**Fig. 4c**,**d** and **Supplementary Fig. 14**). These observations provided direct evidence that AS6 induced the gate-closed conformer and that the *S*-hexyl chain was positioned to interfere with PP2C binding through steric effects.

The functional selectivity of AS*n*

The compounds in the AS*n* series were structurally nearly identical to ABA, with the exception of their 3′-alkyl chains. Although direct evidence was developed here for receptor-mediated physiological effects by these compounds, it is conceivable that activity at other ABA binding sites could have contributed to their effects *in vivo*. Thus, the effects of AS2 and AS6 on two well-characterized, nonreceptor ABA-binding sites were characterized, and, as described above, AS*n* compounds were not potent inhibitors of ABA catabolic CYP707A enzymes. Moreover, endogenous ABA concentrations in *Arabidopsis* seedlings treated with AS2 or AS6 were investigated to examine whether these concentrations were altered by AS*n* compounds. No significant differences ($P > 0.1$ by one-way analysis of variance; $n = 5$ or 6) were observed in ABA concentrations between AS*n* and mock-treated controls (**Supplementary Fig. 15**), suggesting that AS*n* exerted little effect on ABA metabolism. Recently, two ATP-binding cassette (ABC) transporters, AtABCG25 (ref. 42) and AtABCG40 (ref. 43), and the nitrate transporter NPF4.6 (also known as AIT1)[44] were described as ABA transporters. The effect of AS6 on AIT1, whose assay system has been established uniquely among the ABA transporters, was examined, and AS6 was found not to substantially inhibit ABA transport activity by AIT1

when present at equimolar concentrations to ABA; however, it weakly inhibited transport when present in tenfold excess (**Supplementary Fig. 16**). These data suggest that AS6 is not a strong inhibitor of ABA transport activity.

DISCUSSION

A structure-guided design was used to rationally and successfully create an ABA receptor antagonist, demonstrating that this allosteric ligand could be modified relatively easily to yield a PPI inhibitor. Consistent with the present PYR1–AS6 model (**Supplementary Fig. 3**), the AS*n* analog series, prepared by 3′ *S*-alkylation of ABA, yielded agonists when $n < 4$ and yielded antagonists when $n > 4$. Thus, the 3′ position of ABA's ring was found to be a versatile ABA modification site. The present structural, thermodynamic, biochemical and physiological data demonstrated that AS6 bound to PYLs with affinity comparable to ABA and prevented formation of ABA-induced PYL–PP2C complexes by direct steric hindrance of its *S*-hexyl chain. However, AS6 did not completely abolish PYL-PP2C interactions owing to its basal partial agonist activity. Notably, this partial agonist activity *in vitro* did not correspond to partial activation of ABA responses *in vivo*, suggesting that partial reversal of ABA-induced PP2C inhibition was sufficient to block ABA signal transduction *in vivo*. The incomplete inhibition of ABA-induced PYL-PP2C interactions by AS6 might have been sufficient to displace PP2C toward the native substrates, including SnRK2s and OST1. In the PP2C assay, an artificial, small, phosphorylated molecule, *p*-nitrophenylphosphate (*p*NPP), was used as a substrate instead of phosphorylated proteins. PP2C affinity for this small substrate might have been much lower than to native protein substrates[45], in which case, even if a PYL–AS6 complex bound weakly to PP2C, the weak ligand of PP2C should have been easily replaced by native substrates to form stable complexes. Thus, the weak activity of PYL-AS6 *in vitro* might have

been similar to the basal activity of monomeric PYL proteins *in vitro*, which has not been proven with phosphorylated proteins[33,46].

A good deal of the current understanding of ABA's functions *in vivo* has come from analyses of mutants of model organisms that are defective in either ABA signaling or biosynthesis. The present creation and characterization of AS6 now makes feasible studies of ABA signaling in nonmodel organisms. It was shown here using AS6, for example, that blocking of ABA signaling in *R. sativus* increased water loss and, in *L. sativa*, blocked ABA's effects on seed germination. Although these results were not surprising, they highlight the portability of this new tool for answering biological questions in nonmodel systems. Furthermore, the steric strategy for controlling PPIs presented here might be generally applicable to the design of other allosteric modulators of PPIs.

METHODS

Methods and any associated references are available in the online version of the paper.

Accession codes. PDB: The atomic coordinates of the PYR1–AS6 complex have been deposited under accession code 3WG8.

Received30 September 2013; accepted 7 April 2014; published online XX XXX 2014

References

<jrn>1. Kumari, S. & van der Hoorn, R.A.L. A structural biology perspective on bioactive small molecules and their plant targets. *Curr. Opin. Plant Biol.* **14**, 480–488 (2011). </jrn>

<jrn>2. Lumba, S., Cutler, S. & McCourt, P. Plant nuclear hormone receptors: a role for small molecules in protein-protein interactions. *Annu. Rev. Cell Dev. Biol.* **26**, 445–469 (2010). </jrn>

<jrn>3. Santiago, J., Henzler, C. & Hothorm, M. Molecular mechanism for plant steroid receptor activation by somatic embryogenesis co-receptor kinases. *Science* **341**, 889–892 (2013). </jrn>

<jrn>4. Sun, Y. *et al.* Structure reveals that BAK1 as a co-receptor recognizes the BRI1-bound brassinolide. *Cell Res.* **23**, 1326–1329 (2013). </jrn>

<jrn>5. Wells, J.A. & McClendon, C.L. Reaching for high-hanging fruit in drug discovery at protein-protein interfaces. *Nature* **450**, 1001–1009 (2007). </jrn>

<jrn>6. Yoon, J.M. *et al.* Chemical screening of an inhibitory for gibberellin receptors based on a yeast two-hybrid system. *Bioorg. Med. Chem. Lett.* **23**, 1096–1098 (2013). </jrn>

<jrn>7. Hayashi, K. *et al.* Rational design of an auxin antagonist of the SCF^{TIR1} auxin receptor complex. *ACS Chem. Biol.* **7**, 590–598 (2012). </jrn>

<jrn>8. Hayashi, K. *et al.* Small-molecule agonists and antagonists of F-box protein-substrate interactions in auxin perception and signaling. *Proc. Natl. Acad. Sci. USA* **105**, 5632–5637 (2008). </jrn>

<jrn>9. Muto, T. & Todoroki, Y. Brassinolide-2,3-acetonide: a brassinolide-induced rice lamina joint inclination antagonist. *Bioorg. Med. Chem.* **21**, 4413–4419 (2013). </jrn>

<jrn>10.Dupeux, F. *et al.* A thermodynamic switch modulates abscisic acid receptor sensitivity. *EMBO J.* **30**, 4171–4184 (2011). </jrn>

<jrn>11.Hao, Q. *et al.* The molecular basis of ABA-independent inhibition of PP2Cs by a subclass of PYL proteins. *Mol. Cell* **42**, 662–672 (2011). </jrn>

<unknown>12 Hao, Q. *et al.* Functional mechanism of the abscisic acid agonist pyrabactin. *J. Biol. Chem.* **285**, 28946–28952 (2010).</unknown>

<jrn>13.Melcher, K. *et al.* A gate-latch-lock mechanism for hormone signalling by abscisic acid receptors. *Nature* **462**, 602–608 (2009). </jrn>

<jrn>14.Melcher, K. *et al.* Identification and mechanism of ABA receptor antagonism. *Nat. Struct. Mol. Biol.* **17**, 1102–1108 (2010). </jrn>

<jrn>15.Melcher, K., Zhou, X.E. & Xu, H.E. Thirsty plants and beyond: structural mechanisms of abscisic acid perception and signaling. *Curr. Opin. Struct. Biol.* **20**, 722–729 (2010). </jrn>

<jrn>16.Miyazono, K. *et al.* Structural basis of abscisic acid signalling. *Nature* **462**, 609–614 (2009). </jrn>

<jrn>17.Nishimura, N. *et al.* Structural mechanism of abscisic acid binding and signaling by dimeric PYR1. *Science* **326**, 1373–1379 (2009). </jrn>

<jrn>18.Santiago, J. *et al.* The abscisic acid receptor PYR1 in complex with abscisic acid. *Nature* **462**, 665–668 (2009). </jrn>

<jrn>19.Yin, P. *et al.* Structural insights into the mechanism of abscisic acid signaling by PYL proteins. *Nat. Struct. Mol. Biol.* **16**, 1230–1236 (2009). </jrn>

<jrn>20.Zhang, X. *et al.* Complex structures of the abscisic acid receptor PYL3/RCAR13 reveal a unique regulatory mechanism. *Structure* **20**, 780–790 (2012). </jrn>

<jrn>21.Cutler, S.R., Rodriguez, P.L., Finkelstein, R.R. & Abrams, S.R. Abscisic acid: emergence of a core signaling network. *Annu. Rev. Plant Biol.* **61**, 651–679 (2010). </jrn>

<jrn>22.McCarty, D.R. Genetic-control and integration of maturation and germination pathways in seed development. *Annu. Rev. Plant Physiol.* **46**, 71–93 (1995). </jrn>

<jrn>23.Ma, Y. *et al.* Regulators of PP2C Phosphatase activity function as abscisic acid sensors. *Science* **324**, 1064–1068 (2009).</jrn>

<jrn>24.Park, S.Y. *et al.* Abscisic acid inhibits type 2C protein phosphatases via the PYR/PYL family of START proteins. *Science* **324**, 1068–1071 (2009).</jrn>

<jrn>25.Soon, F.F. *et al.* Molecular mimicry regulates ABA signaling by SnRK2 kinases and PP2C phosphatases. *Science* **335**, 85–88 (2012). </jrn>

<jrn>26.Fujii, H. *et al. In vitro* reconstitution of an abscisic acid signalling pathway. *Nature* **462**, 660–664 (2009). </jrn>

<jrn>27.Ng, L.M. *et al.* Structural basis for basal activity and autoactivation of abscisic acid (ABA) signaling SnRK2 kinases. *Proc. Natl. Acad. Sci. USA* **108**, 21259–21264 (2011). </jrn>

<jrn>28.Brandt, B. *et al.* Reconstitution of abscisic acid activation of SLAC1 anion channel by CPK6 and OST1 kinases and branched ABI1 PP2C phosphatase action. *Proc. Natl. Acad. Sci. USA* **109**, 10593–10598 (2012). </jrn>

<jrn>29.Geiger, D. *et al.* Activity of guard cell anion channel SLAC1 is controlled by drought-stress signaling kinase-phosphatase pair. *Proc. Natl. Acad. Sci. USA* **106**, 21425–21430 (2009). </jrn>

<jrn>30.Umezawa, T. *et al.* Type 2C protein phosphatases directly regulate abscisic acid–activated protein kinases in *Arabidopsis*. *Proc. Natl. Acad. Sci. USA* **106**, 17588–17593 (2009). </jrn>

<jrn>31.Xue, S. *et al.* Central functions of bicarbonate in S-type anion channel activation and OST1 protein kinase in CO2 signal transduction in guard cell. *EMBO J.* **30**, 1645–1658 (2011). </jrn>

<jrn>32.Santiago, J. *et al.* Modulation of drought resistance by the abscisic acid receptor PYL5 through inhibition of clade A PP2Cs. *Plant J.* **60**, 575–588 (2009). </jrn>

<jrn>33.Antoni, R. *et al.* PYRABACTIN RESISTANCE1-LIKE8 plays an important role for the regulation of abscisic acid signaling in root. *Plant Physiol.* **161**, 931–941 (2013). </jrn>

<jrn>34.Gonzalez-Guzman, M. *et al.* *Arabidopsis* PYR/PYL/RCAR receptors play a major role in quantitative regulation of stomatal aperture and transcriptional response to abscisic acid. *Plant Cell* **24**, 2483–2496 (2012). </jrn>

<jrn>35.Okamoto, M. *et al.* Activation of dimeric ABA receptors elicits guard cell closure, ABA-regulated gene expression, and drought tolerance. *Proc. Natl. Acad. Sci. USA* **110**, 12132–12137 (2013). </jrn>

<unknown>36 Todoroki, Y. & Hirai, N. Abscisic acid analogs for probing the mechanism of abscisic acid reception and inactivation. *Stud. Nat. Prod. Chem.* **27**, 321–360 (2002).</unknown>

<jrn>37.Ji, X. *et al.* Control of abscisic acid catabolism and abscisic acid homeostasis is important for reproductive stage stress tolerance in cereals. *Plant Physiol.* **156**, 647–662 (2011). </jrn>

<jrn>38.Todoroki, Y. & Ueno, K. Development of specific inhibitors of CYP707A, a key enzyme in the catabolism of abscisic acid. *Curr. Med. Chem.* **17**, 3230–3244 (2010). </jrn>

<jrn>39.Kushiro, T. *et al.* The *Arabidopsis* cytochrome P450 CYP707A encodes ABA 8′-hydroxylases: key enzymes in ABA catabolism. *EMBO J.* **23**, 1647–1656 (2004). </jrn>

<jrn>40.Saito, S. *et al. Arabidopsis CYP707A*s encode (+)-abscisic acid 8′-hydroxylase, a key enzyme in the oxidative catabolism of abscisic acid. *Plant Physiol.* **134**, 1439–1449 (2004). </jrn>

<jrn>41.Ueno, K. *et al.* Differences between the structural requirements for ABA 8 '-hydroxylase inhibition and for ABA activity. *Bioorg. Med. Chem.* **13**, 3359–3370 (2005). </jrn>

<jrn>42.Kuromori, T. *et al.* ABC transporter AtABCG25 is involved in abscisic acid transport and responses. *Proc. Natl. Acad. Sci. USA* **107**, 2361–2366 (2010). </jrn>

<jrn>43.Kang, J. *et al.* PDR-type ABC transporter mediates cellular uptake of the phytohormone abscisic acid. *Proc. Natl. Acad. Sci. USA* **107**, 2355–2360 (2010). </jrn>

<jrn>44.Kanno, Y. *et al.* Identification of an abscisic acid transporter by functional screening using the receptor complex as a sensor. *Proc. Natl. Acad. Sci. USA* **109**, 9653–9658 (2012). </jrn>

<jrn>45.Fjeld, C.C. & Denu, M.J. Kinetic analysis of human serine/threonine protein Phosphatase 2Cα. *J. Biol. Chem.* **274**, 20336–20343 (1999). </jrn>

<jrn>46.Pizzio, G.A. *et al.* The PYL4194T mutant uncovers a key role of PYR1-LIKE4/PROTEIN PHOSPHATASE 2Cα interaction for abscisic acid signaling and plant drought resistance. *Plant Physiol.* **163**, 441–455 (2013). </jrn>

Acknowledgments

We thank T. Nakagawa for providing pGWB vectors and Toray Industries Inc., Tokyo, Japan, for the gift of (+)-ABA. This work was supported in part by the Japanese Society for the Promotion of Science (JSPS) Postdoctoral Fellowships for Research Abroad (to M.O.), JSPS KAKENHI (Grant-in-Aid for Young Scientists 26711018 to M.O.) and the US National Science Foundation (Integrative Organismal Systems 0820508 to S.R.C.).

Author contributions

J.T., M.O. and Y.T. conceived and J.T., M.O., S.R.C. and Y.T. designed the research. J.T., M.O., T.A., T.M., S.Y., M. Sue, M. Seo, Y.K., T.K., A.E., E.N., S.R.C. and Y.T. performed the research and/or analyzed data. J.T., M.O., S.R.C. and Y.T. co-wrote the manuscript with the assistance of M. Sue, M. Seo, N.H. and T.O.

Competing financial interests

The authors declare no competing financial interests.

Additional information

Supplementary information and chemical compound information is available in the online version of the paper.

Reprints and permissions information is available online at http://www.nature.com/reprints/index.html.

Correspondence and requests for materials should be addressed to Y.T.

Figure 1 | Synthesis of AS*n* compounds and AS*n* effects on *Arabidopsis* seed germination. (**a**) Synthesis of AS*n* compounds (*n* = 2–12). (**b**) Seed germination rate in the presence of AS*n* at 24 h after stratification (*n* = 3; error bars represent s.d.). (**c**) Seed germination rate in presence of 0.3 μM ABA and 1.0 μM AS*n* at 36 h after stratification (*n* = 3; error bars represent s.d.).

Figure 2 | Effects of AS*n* compounds on expression of *Arabidopsis* ABA-responsive genes. (**a**) Expression of ABA-responsive genes after chemical treatments. Chemical concentrations were tested at 0 μM, 1 μM, 5 μM, 10 μM, 25 μM and 50 μM. (**b**) Spatial expression pattern of *MAPKKK18* after 5 μM chemical treatment. (**c**) Expression of ABA-responsive genes after cotreatment with ABA and AS*n* or PyrA. AS*n* compounds were tested at 0 μM, 1 μM, 5 μM, 10 μM, 25 μM and 50 μM in presence of 10 μM ABA. (**d**) Spatial expression pattern of *MAPKKK18* after cotreatment with 5 μM ABA and 50 μM AS*n* or PyrA. In **a**–**d**, 6-d-old *Arabidopsis* wild-type (Columbia accession) and promoter *MAPKKK18::GUS* transgenic seedlings incubated in solution containing chemicals in 0.5x MS and 0.5% sucrose for 6 h were used. In **a** and **c**, *n* = 3, and error bars represent s.d. In **b** and **d**, scale bars represent 0.5 mm.

Figure 3 | Effects of AS*n* on HAB1 inhibition by ABA receptors. (**a**) Chemical-dependent inhibition of HAB1 by various ABA receptors. Assays were conducted in presence of 25 μM of each test chemical. Antagonistic effect of 50 μM AS*n* compounds (**b**) or various concentrations of AS*n* compounds (**c**) on HAB1 inhibition by various ABA receptors in presence of ABA. (**b**) Assays conducted in presence of both 5 μM ABA and 50 μM AS*n* compounds. (**c**) AS*n* compounds were tested at 0 μM, 0.5 μM, 2.5 μM, 5 μM, 10 μM, 25 μM, 50 μM and 100 μM, whereas ABA was used at 5 μM in reactions. HAB1 activity in absence of receptor protein and chemical are shown as 100% of enzyme activity. PYL and HAB1 proteins were used at the same molar ratio at 60 pmol; $n = 3$; error bars represent s.d.

Figure 4 | Crystal structure of PYR1–AS6 complex. (**a**) Overall structure of AS6-bound PYR1. AS6 is shown as purple sticks. (**b**) Superposition of the PYR1–AS6 complex (cyan) and PYR1–ABA complex (gray, PDB code 3K90) at the ligand binding pocket. (**c**,**d**) Superposition of the PYR1–AS6 complex and the PYR1–ABA–HAB1 (orange, PDB code 3QN1) complex. The gate loop of the PYR1–AS6 complex adopted a closed conformation, and the AS6 *S*-hexyl chain passed through the 3′ tunnel to protrude over the PYR1 surface. In **c**, Val163 in the α3 helix and Val83 at the N terminus of the gate loop region are located at the top and bottom of the tunnel, respectively, and are highlighted in spheres. In **d**, the *S*-hexyl chain tip collided with HAB1 Val393, which is well conserved among PP2Cs (**d**).

Online Methods

Molecular modeling of a PYR1–AS6 complex.

The initial structure of AS6 was built by adding an *S*-hexyl chain onto the 3′-carbon of ABA in GaussView 5 (ref. 47) before it was fully optimized through density functional theory, using the Becke three parameter hybrid functional (B3LYP) method and the 6-31G (d) basis set in Gaussian 09 (ref. 48). The RESP charge distributions of AS6 were obtained using R.E.D.

Server[49], a web service for deriving RESP charges. Hydrogen molecules were added to a gate-closed conformer of PYR1, and water molecules were added to the PYR1–ABA complex (PDB code 3K3K) using the AddH function in Chimera. The AS6 molecule was manually inserted into the ABA-binding site in this modified PYR1, and the PYR1–AS6 complex was minimized using the Tinker program[50] with amber99 and modified amber gaff parameters with the GB/SA model.

Arabidopsis seed germination assay.

Twenty-five to forty seeds (Columbia accession) were sterilized successively with soaking in 70% aqueous ethanol (EtOH, v/v) for 30 min and reagent-grade EtOH for 1 min. They were then soaked in 250 μl of a test solution and incubated in darkness at 5 °C for 3 d. The stratified seeds in the test solution were transferred onto two pieces of filter paper in 24-well plates and allowed to germinate under continuous illumination at 22 °C for 24 h or 36 h. All of the assays were conducted at least three times.

Arabidopsis early growth assay.

Twenty to thirty seeds (Columbia accession) were sterilized successively with 70% aqueous EtOH (v/v) for 30 min and reagent-grade EtOH for 1 min. They were then were soaked in 100 μl of a test medium liquid agar in 96-well plates and allowed to germinate and grow at 22 °C and under continuous illumination for 5 d or 10 d. All of the assays were conducted at least three times.

Lettuce seed germination and early growth assay.

Twenty-five seeds (*Lactuca sativa* L. cv. Grand Rapids) were placed in a dish on two sheets of filter paper soaked in 2 ml of a test solution and allowed to germinate and grow at 22 °C and under continuous illumination for 14 d. The germination rate was determined as the time when

the germination rate of the control plant was 50% or the germination rate of only ABA-treated plants was 40%. All of the assays were conducted at least three times.

Radish seedling water-loss assay.

Radish seeds (*Raphnus sativus* L. var. raphanistroides (Makino) Sinsk.) were soaked in water at 25 °C in darkness for 2 d and allowed to germinate and grow under continuous illumination for 5 d. Seven-day old seedlings were placed in a plastic tube containing 15 ml of a test solution and incubated at 25 °C and under continuous illumination for 12 h. The plants were transferred to empty tubes and exposed to drought stress under same conditions for 4 h. Water content was expressed as a relative reduction rate normalized to a control (untreated) value of 100%.

Thermal imaging.

Seven-day old radish seedlings (sp. and var. as above) grown under continuous illumination at 25 °C were placed in plastic tubes containing 15 ml of a test solution and were incubated in darkness at 25 °C for 12 h. Thermal images were obtained using Testo 881-2 thermography (Testo, Inc., Sparta, NJ, USA). Images were saved in a computer memory card and analyzed using the IRSoft software (Testo, Inc.).

CYP707A3 inhibition assay.

Reaction mixtures containing 25 μg ml^{-1} of CYP707A3 microsomes (coexpressed with AR2 in *E. coli*)[51], ABA (final concentration 1–64 μM), inhibitors (0 for control, 50–100 μM in 5 μl dimethylformamide (DMF)) and 130 μM NADPH in 100 mM potassium phosphate buffer (pH 7.25) were incubated at 30 °C for 10 min. Reactions were initiated by adding NADPH, stopped by addition of 50 μl of 1 M NaOH and then acidified with 100 μl of 1 M HCl. Reaction products were extracted by loading the mixture onto an Oasis HLB cartridge (1 ml, 30 mg; Waters Corp., Milford, MA, USA) and were washed with 1 ml of 10% MeOH in H_2O (v/v) containing 1% AcOH (v/v). The enzyme products were then eluted with 1 ml of MeOH containing 1% AcOH,

and the eluate was concentrated *in vacuo*. The dried sample was then dissolved in 50 μl of MeOH, and a 20-μl volume was subjected to HPLC (Prominence; Shimadzu Corp., Kyoto, Japan). HPLC conditions were as follows: the octadecylsilyl (ODS) column was composed of Hydrosphere C18 (150 × 6.0 mm, YMC Co., Ltd., Kyoto, Japan), solvent comprised 17% acetonitrile (MeCN) in H_2O containing 0.05% AcOH (v/v), the flow rate was 1.0 ml min^{-1}, and detection was at 254 nm. Enzyme activity was evaluated by determining the amount of phaseic acid in control experiments before each set of measurements. The inhibition constants for AS2 and AS6 were determined using the Enzyme Kinetics module of SigmaPlot 10 software (Systat Software, Inc., San Jose, CA, USA) after determining the inhibition mode by plotting the reaction velocity in the presence and absence of inhibitor on a double-reciprocal plot. All of the tests were conducted at least three times.

qRT-PCR analysis.

Total RNA was isolated using Plant RNA Purification reagent (Invitrogen Corp., Carlsbad, CA, USA), according to the manufacturer's protocol. cDNA was synthesized using the QuantiTec reverse transcription kit (Qiagen GmbH, Hilden, Germany). Real-time PCR using Maxima SYBR Green/Fluorescein qPCR Master Mix (Thermo Fisher Scientific, Inc., Pittsburgh, PA, USA) was performed with the iQ5 real-time PCR detection system (Bio-Rad Laboratories, Inc., Hercules, CA, USA). The relative amount of target mRNA was based on a standard curve and normalized to the relative amount of internal control mRNA. Biological triplicate experiments were performed, and primer sets were used as previously described[35]. Pyrabactin (98%) was purchased from Sigma-Aldrich, Inc. (St. Louis, MO, USA).

GUS staining assay.

For ABA-responsive reporter gene analyses, transgenic *Arabidopsis* expressing β-glucuronidase (GUS) under the control of the AtMAPKKK18 promoter were used, as

previously described[35]. Six-day-old seedlings were used in this study, and GUS staining was performed in a reaction buffer composed of 50 mM sodium phosphate buffer, pH 7.0, 0.05% Tween-20, 2.5 mM potassium ferrocyanide, 2.5 mM potassium ferricyanide and 1 mM X-gluc. After incubation at 37 °C, the reaction was stopped by EtOH addition, and green pigments in the sample were extracted into EtOH with incubation at 65 °C.

PP2C enzyme assay.

For production of PP2C protein, GST-HAB1 was cloned into pGex-2T, as previously described[24]. For ABA receptor proteins, PYL cDNAs were cloned into pET28 vector, whereas PYL11 cDNA was cloned into pMAL-c vector[24,35]. Functional PYL7 and PYL12 were not obtained in this expression system using pET28 or pMAL-c vectors. HAB1 and PYL proteins were expressed and purified, as previously described[35]. Briefly, plasmids were transformed into BL21[DE3]pLysS, the resulting transformant cells were precultured overnight in 10 ml LB medium, and then cells were grown in 800 ml medium at 30 °C to an OD_{600} ~0.5. Protein expression was induced by IPTG addition, and inductions were conducted at 15 °C for 16 h. Cells were harvested, frozen, thawed and sonicated, and the constituent proteins were purified by affinity column chromatography. Purified proteins were preincubated in 80 μl of buffer containing 12.5 mM $MnCl_2$, 0.125% 2-mercaptoethanol and test compound at 22 °C for 30 min. After adding 20 μl of substrate buffer (165 mM Tris-acetate, pH 7.9, 330 mM potassium acetate, 0.1% BSA and 250 mM *p*NPP), reactions were immediately monitored for hydrolysis of *p*NPP at 405 nm. The PP2C assay was performed using 60 pmol each of PP2C and PYL.

Pull-down assay.

Here, 100 μg and 20 μg of purified GST-HAB1 and His_6-tagged PYLs, respectively, were incubated in 200 μl of Tris-buffered saline (TBS) containing 100 μg BSA, 0.025% 2-mercaptoethanol, 10 mM $MnCl_2$ and 10 mg PrepEase His-tagged protein purification resin

(Affymetrix, Inc., Santa Clara, CA, USA) in the presence or absence of test compounds with gentle shaking at 4 °C for 60 min. The resin was then washed five times with TBS containing 0.025% 2-mercaptoethanol and 10 mM $MnCl_2$, while held on ice. The bound proteins were eluted in 60 μl of SDS-sample buffer with 250 mM imidazole and denatured at 95 °C for 5 min. Then, 10 μl of eluate was loaded on a 13% SDS-PAGE gel, and proteins were detected after development by Coomassie brilliant blue staining.

Isothermal titration calorimetry.

AS*n*-binding studies were performed by isothermal titration calorimetry (ITC) using an iTC_{200} calorimeter (Microcal, GE Healthcare Bio-Sciences AB) and were conducted at 20 °C and with a solvent of 100 mM phosphate buffer, pH 8.0. His_6-tagged PYL5 or His_6-tagged PYL10 were assayed at a concentration of 40 μM and 50 μM, respectively, with AS6 and ABA stock solutions in the injection syringe at tenfold higher concentrations than the proteins. All of the titrations were carried out via a series of 20 injections of 1.25 μl each. The data were corrected by subtracting the mixing enthalpies for the AS6 or ABA solutions into protein-free solutions and fitted by Origin for ITC (GE Healthcare Bio-Sciences AB) with a 1/1 binding model.

Protein preparation and crystallization.

For crystallization of the PYR1–AS6 complex, PYR1 was cloned into a pET-28 vector, as previously described[24]. The plasmid was then transformed into *E. coli* strain BL21-CodonPlus (DE3)-RIPL (Agilent Technologies, Santa Clara, CA, USA), and transformed cells were incubated at 30 °C to an OD_{600} ~0.5. Protein expression was induced by IPTG addition and incubation at 16 °C for 16 h, after which cells were harvested, frozen, thawed and sonicated. Protein was then purified from this preparation using a Ni-Sepharose resin (GE Healthcare Bio-Sciences AB) and eluted with binding buffer (150 mM phosphate, pH 8.0, and 300 mM NaCl) supplemented with 250 mM imidazole. The protein was further purified using a

Resource Q column (GE Healthcare Bio-Sciences AB) and eluted with binding buffer (10 mM Tris-HCl, pH 8.0) supplemented with 150 mM NaCl. Peak fractions were concentrated using an Amicon Ultrafilter (30,000 MWCO, Millipore Corp., Billerica, MA, USA).

Crystallization was performed using the hanging-drop vapor-diffusion method at 20 °C, and crystallization buffer comprised 100 mM HEPES (pH 7.5) with 20% (v/v) PEG 10,000 as the reservoir buffer. Drops of protein solution (1.5 μl, 10 mg ml^{-1}) containing 1 mM AS6 were mixed with 1.5 μl of reservoir buffer. Crystals were flash-frozen at 100 K under a cold stream of nitrogen gas without cryoprotectant.

Data collection, structure determination and refinement.

Diffraction data of PYR1 cocrystallized with AS6 were collected on beamline 17A at the Photon Factory (Tsukuba, Japan), and data sets were processed with the program HKL2000 (ref. 52). The initial structure of the complex was solved by molecular replacement using the program MOLREP[53,54] in the CCP4 suite[55] with the PYR1 coordinates (PDB code 3K90) as a target model. Refinements were carried out with the program REFMAC5 (ref. 56) in the CCP4 suite, and the restraint file for the AS6 molecule was obtained at thePRODRG server[57]. Manual model building was performed using Coot[58], and the structure was refined at 2.3 Å to R_{work}/R_{free} factors of 23.8%/28.1%. The statistics for data collection and refinement are provided in **Supplementary Table 5**.

Quantitative analysis of endogenous ABA.

Measurement of endogenous ABA has been described elsewhere[59,60]. Briefly, 10-d-old plants (0.5–1 g) were incubated for 6 h in a 10 μM AS2 or AS6 solution or water as a control . These plants were homogenized in 80% aqueous acetone (v/v) containing 0.1 mg/ml 2,6-di-*tert*-butyl-4-methylphenol as an antioxidant. A 5.0 ng of [3′,5′,5′,7',7',7'-$^{2}H_{6}$]ABA (d_6-ABA), as the internal standard, was added to a homogenized sample before the following

extraction procedure. The homogenate was centrifuged at 5,000*g* and 4 °C for 15 min, and the supernatant was reduced to the aqueous phase *in vacuo*. After washing with hexane, the pH was adjusted to 2 using 0.5 M phosphoric acid, and ABA was extracted into EtOAc. The solvent was removed from this extract *in vacuo*, and the residue was dissolved in 110 μl of 10% MeOH containing 0.1% AcOH (v/v) and introduced into a HPLC. HPLC conditions were as follows: ODS column with Hydrosphere C18 (150 × 6.0 mm, YMC Co.), a solvent gradient program of MeOH containing 0.1% AcOH (35–60% MeOH over 30 min), flow rate of 1.0 ml min^{-1} and detection at 254 nm. The fraction containing ABA standard was collected, dried *in vacuo* and then methylated with trimethylsilyldiazomethane. The resulting methylated samples were dissolved in 10 μl of EtOAc and analyzed by gas chromatography-MS on a QP5050A system (Shimadzu Corp., Kyoto, Japan) using an Equity-5 column (Supelco Inc., Bellefonte, PA, USA; 0.25 mm i.d. × 30 m, 0.25-μm film thickness) and helium carrier gas at linear and total flow rates of 35.6 cm s^{-1} and 50 ml min^{-1}, respectively The column flow rate was set at 1.0 ml min^{-1}, and splitless injection mode was used with a 2-min sampling time at 200 kPa. The programmed column temperature was a step gradient of 60 °C for 2 min, 60–270 °C at 10 °C min^{-1} and then 270 °C for 35 min. The system was set with a 70-eV electron potential and 0.5-s signal sampling rate, and qualitative analysis was performed in selected-ion monitoring mode. Samples (2.5 μl) of material were injected onto the column and d_0-ABA and d_6-ABA methyl esters detected with retention times of 22.54 min and 22.49 min, respectively. The mass chromatogram peak area of the $[M\text{-}C_5H_{12}O]^+$ ion (*m/z* 190) derived from d_0-ABA methyl ester was compared to that of d_6-ABA methyl ester (*m/z* 194). Concentrations were calculated using a linear regression equation based on different concentrations of the methylated standards ABA and d_6-ABA. Identification of ABA methyl ester in samples was conducted in total ion monitoring mode through comparison of the fragmentation pattern with that of the standard.

Statistical analyses.

All statistical analyses were performed using R version 3.0.2 software, and Grubbs' test was used to detect outliers. Normal distributions and assumptions regarding variance homogeneities in ABA concentrations from each treatment were checked using the Shapiro-Wilk test and Bartlett's test, respectively. Differences in ABA concentrations between treatments were tested using one-way ANOVA.

Transport assay.

ABA transport activities of NPF4.6/AIT1 in a yeast system were determined by directly analyzing ABA taken into cells by LC/MS/MS, as described previously, but with some modifications[42]. Potassium phosphate buffer at pH 5.8, instead of pH 7.5, was used for the assays. ABA was extracted from yeast cells at –30 °C overnight in 1 ml of 80% aqueous acetone containing 1% acetic acid (v/v), with d_6-ABA as an internal standard. Supernatants were collected after centrifugation, and acetone was evaporated using a SpeedVac (Thermo Fisher Scientific Inc.) to obtain aqueous extracts containing acetic acid. Solutions were adjusted to 1 ml with 1% acetic acid and applied to Oasis WAX cartridge columns (30 mg, 1 ml; Waters Corp.) prewashed successively with 1 ml of MeCN and methanol, regenerated with 0.5 ml of 0.1 M NaOH and equilibrated with 1 ml of 1% acetic acid. After washing successively with 3-ml volumes of 1% acetic acid and methanol, the fractions containing ABA were eluted with 2 ml of 80% MeCN containing 1% acetic acid (v/v). The eluates were taken to dryness and dissolved in 0.5 ml of chloroform containing 49% ethyl acetate and 1% acetic acid (v/v). They were then loaded on Sep-Pak silica (100 mg; Waters Corp.) cartridge columns prewashed with 3 ml of chloroform and equilibrated with 1 ml of chloroform containing 1% acetic acid. Fractions containing ABA were eluted with 2 ml of chloroform containing 49% ethyl acetate and 1% acetic acid (v/v). The samples were next taken to dryness and dissolved in 20 μl of water containing 1% acetic acid (v/v) before injection into the LC/MS/MS. A Nexera

(Shimadzu Corp., Kyoto, Japan)/Triple TOF 5600 (AB SCIEX, Framingham, MA, USA) system equipped with an ACQUITY UPLC BEH phenyl column (Waters Corp.) was used to quantify ABA, as described previously[42], except that the desolvation temperature was 600 °C instead of 700 °C.

<bok>47. GaussView. Version 5, (Dennington, R., Keith, T. & Millam, J., Semichem Inc., Shawnee Mission, Kansas, USA, 2009)</bok>

<bok>48. Gaussian 09, Revision A.02, (Frisch, M. J. *et al*., Gaussian, Inc., Wallingford, Connecticut, USA, 2009)</bok>

<jrn>49. Vanquelef, E. *et al.* R.E.D. Server: a web service for deriving RESP and ESP charges and building force field libraries for new molecules and molecular fragments. *Nucleic Acids Res.* **39**, W511–W517 (2011) http://q4md-forcefieldtools.org/REDS/. </jrn>

<bok>50. TINKER. Ver. 6.0. (Ponder, J.W., Washington University School of Medicine, St. Louis, Missouri, USA, 2011).</bok>

<jrn>51. Okazaki, M. *et al.* Abscinazole-E2B, a practical and selective inhibitor of ABA 8′-hydroxylase CYP707A. *Bioorg. Med. Chem.* **20**, 3162–3172 (2012). </jrn>

<jrn>52. Otwinowski, Z. & Minor, W. Processing of X-ray diffraction data collected in oscillation mode. *Methods Enzymol.* **276**, 307–326 (1997). </jrn>

<jrn>53. Evans, P. Scaling and assessment of data quality. *Acta Crystallogr. D Biol. Crystallogr.* **62**, 72–82 (2006).</jrn>

<jrn>54. Vagin, A. & Teplyakov, A. *MOLREP*: an automated program for molecular replacement. *J. Appl. Crystallogr.* **30**, 1022–1025 (1997). </jrn>

<jrn>55. Winn, M.D. *et al.* Overview of the *CCP4* suite and current developments. *Acta Crystallogr. D Biol. Crystallogr.* **67**, 235–242 (2011).</jrn>

<jrn>56.Murshudov, G.N., Vagin, A. & Dodsen, E.J. Refinement of macromolecular structures by the maximum-likelihood method. *Acta Crystallogr. D Biol. Crystallogr.* **53**, 240–255 (1997).</jrn>

<jrn>57.Schüttelkopf, A.W. & van Aalten, D.M.F. *PRODRG*: a tool for high-throughput crystallography of protein-ligand complexes. *Acta Crystallogr. D Biol. Crystallogr.* **60**, 1355–1363 (2004).</jrn>

<jrn>58.Emsley, P., Lohkamp, B., Scott, W.G. & Cowtan, K. Features and development of *Coot. Acta Crystallogr. D Biol. Crystallogr.* **66**, 486–501 (2010). </jrn>

<jrn>59.Saito, S. *et al.* A plant growth retardant, uniconazole, is a potent inhibitor of ABA catabolism in *Arabidopsis. Biosci. Biotechnol. Biochem.* **70**, 1731–1739 (2006). </jrn>

<jrn>60.Kondo, S., Ponrod, W., Kanlayanarat, S. & Hirai, N. Abscisic acid metabolism during fruit development and maturation of mangosteens. *J. Am. Soc. Hortic. Sci.* **127**, 737–741 (2002).</jrn>

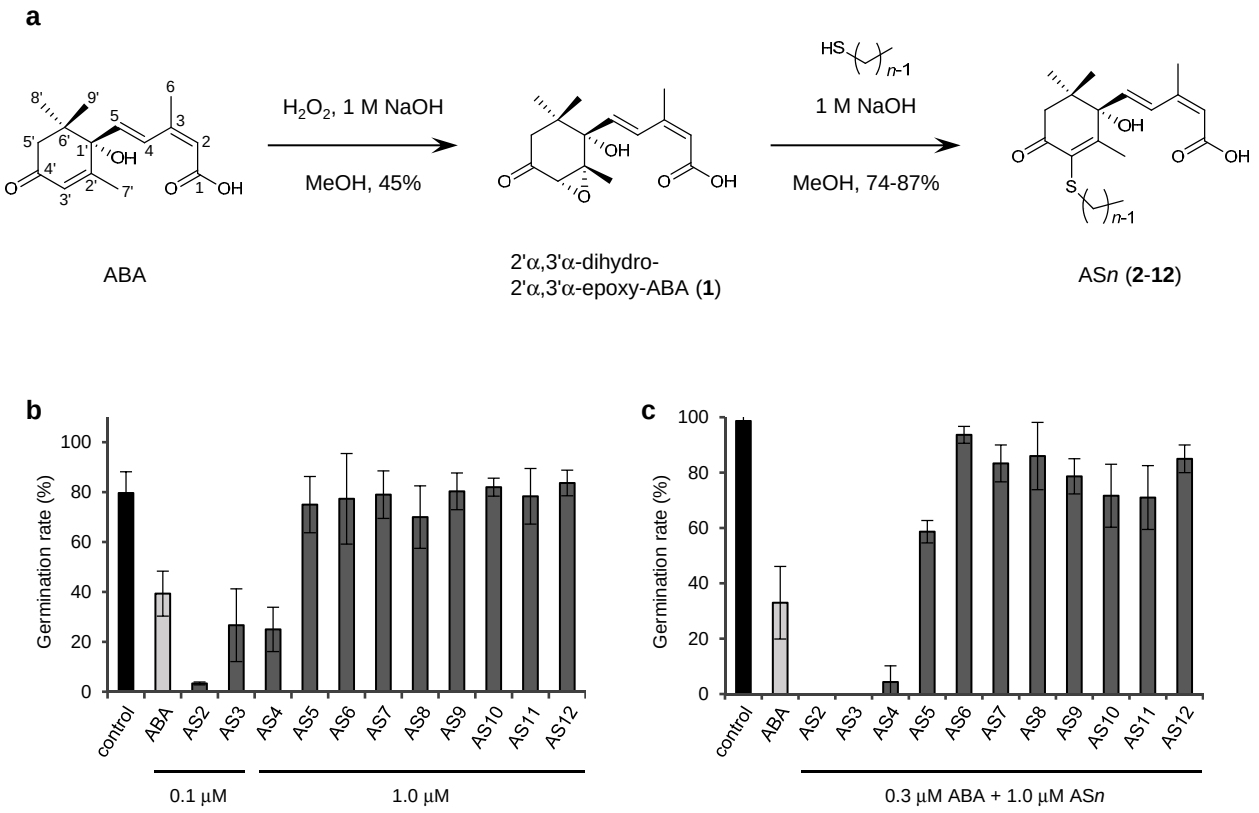

Figure 1 | Synthesis of AS*n* compounds and AS*n* effects on *Arabidopsis* seed germination. (**a**) Synthesis of AS*n* compounds (*n*=2-12). (**b**) Seed germination rate in the presence of AS*n* at 24 h after stratification (*n*=3; error bars represent, s.d.). (**c**) Seed germination rate in presence of 0.3 μM ABA and 1.0 μM AS*n* at 36 h after stratification (*n*=3; error bars represent, s.d.).

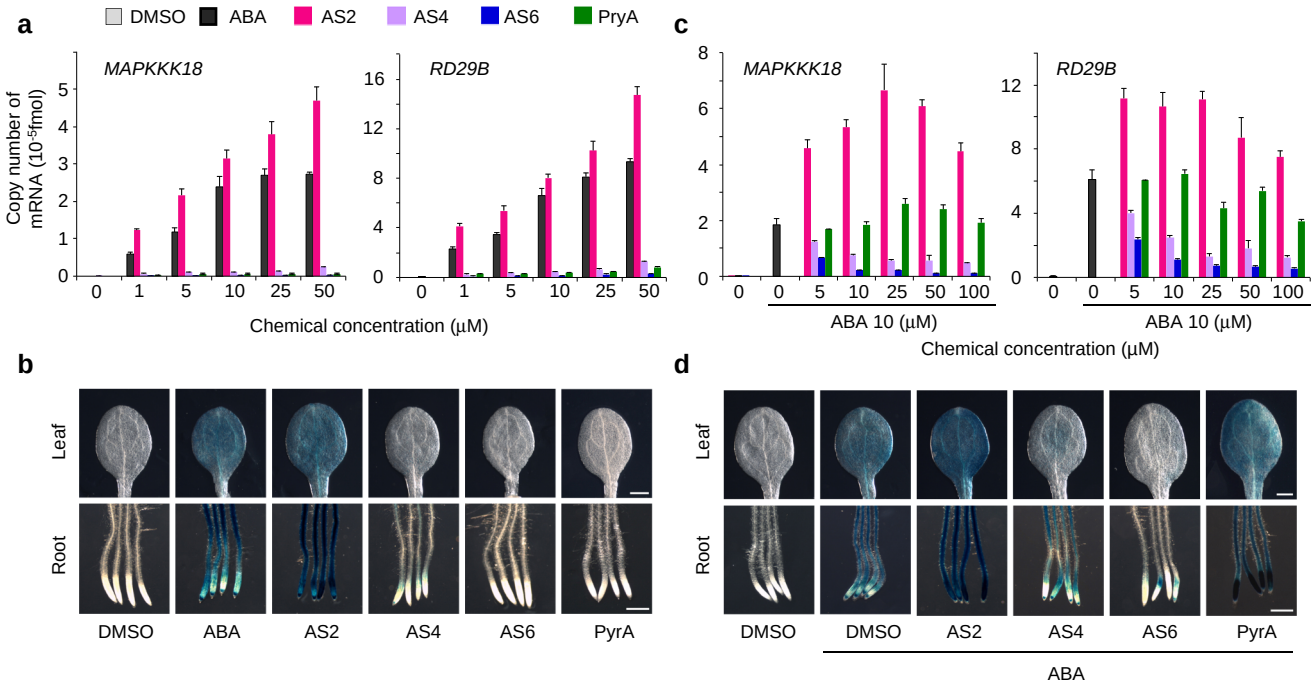

Figure 2 | Effects of AS*n* compounds on expression of *Arabidopsis* ABA-responsive genes. (**a**) Expression of ABA-responsive genes after chemical treatments. Chemical concentrations were tested at 0 μM, 1 μM, 5 μM, 10 μM, 25 μM and 50 μM. (**b**) Spatial expression pattern of *MAPKKK18* after 5 μM chemical treatment. (**c**) Expression of ABA-responsive genes after cotreatment with ABA and AS*n* or PyrA. AS*n* compounds were tested at 0 μM, 1 μM, 5 μM, 10 μM, 25 μM and 50 μM in presence of 10 μM ABA. (**d**) Spatial expression pattern of *MAPKKK18* after cotreatment with 5 μM ABA and 50 μM AS*n* or PyrA. In **a**–**d**, 6-d-old *Arabidopsis* wild-type (Columbia accession) and promoter *MAPKKK18::GUS* transgenic seedlings incubated in solution containing chemicals in 0.5x MS and 0.5% sucrose for 6 h were used. In **a** and **c**, *n* = 3, and error bars represent s.d. In **b** and **d**, scale bars represent 0.5 mm.

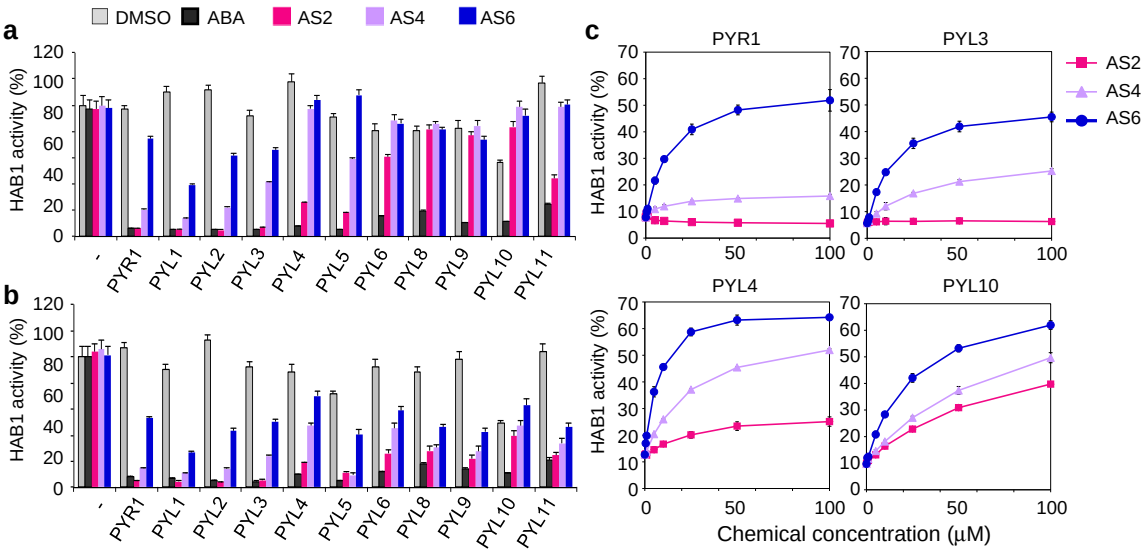

Figure 3 | Effects of AS*n* on HAB1 inhibition by ABA receptors. (**a**) Chemical-dependent inhibition of HAB1 by various ABA receptors. Assays were conducted in presence of 25 μM of each test chemical. Antagonistic effect of 50 μM AS*n* compounds (**b**) or various concentrations of AS*n* compounds (**c**) on HAB1 inhibition by various ABA receptors in presence of ABA. (**b**) Assays conducted in presence of both 5 μM ABA and 50 μM AS*n* compounds. (**c**) AS*n* compounds were tested at 0 μM, 0.5 μM, 2.5 μM, 5 μM, 10 μM, 25 μM, 50 μM and 100 μM, whereas ABA was used at 5 μM in reactions. HAB1 activity in absence of receptor protein and chemical are shown as 100% of enzyme activity. PYL and HAB1 proteins were used at the same molar ratio at 60 pmol; *n* = 3; error bars represent s.d.

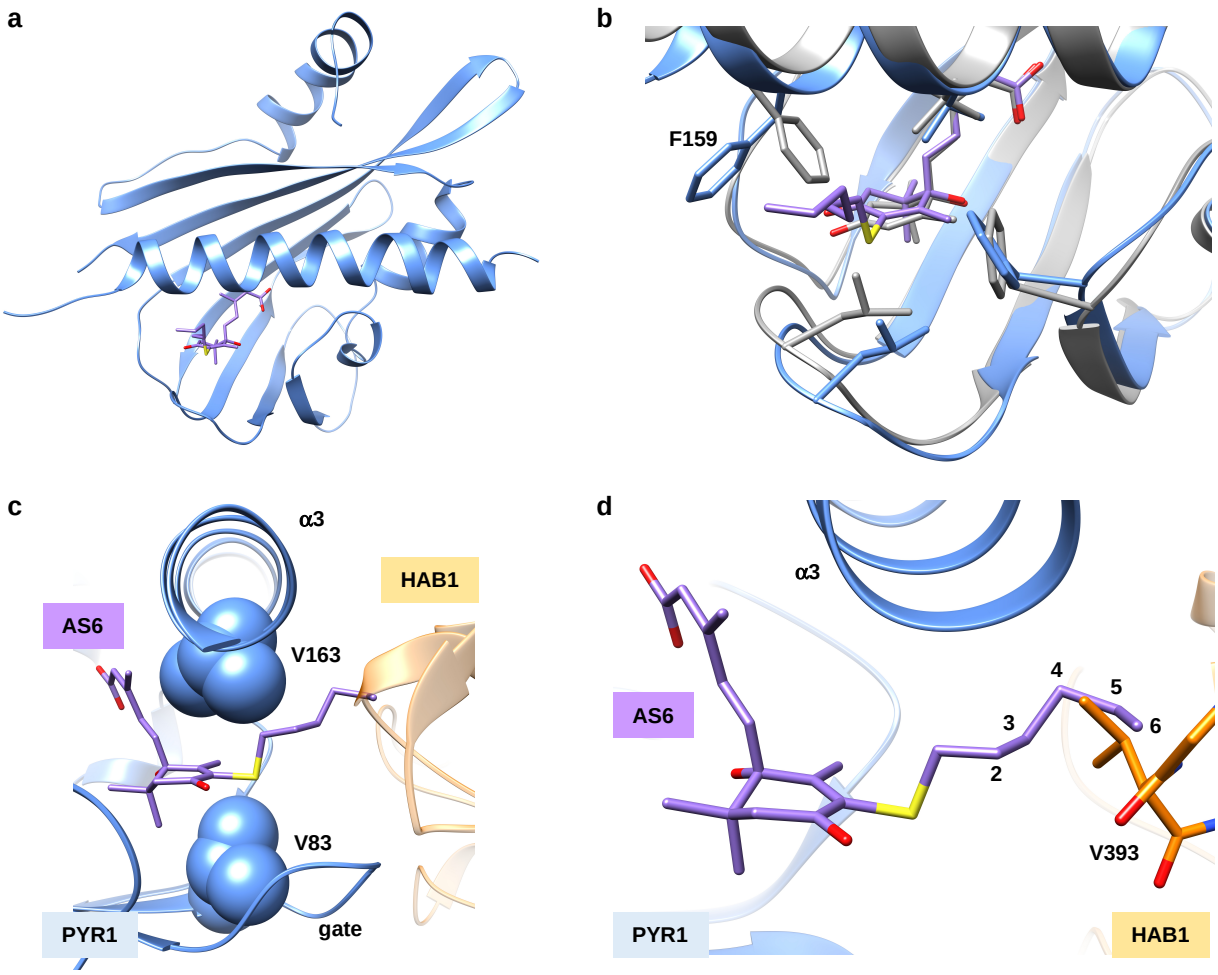

Figure 4 | Crystal structure of PYR1-AS6 complex. (**a**) Overall structure of AS6-bound PYR1. AS6 is shown as purple sticks. (**b**) Superposition of the PYR1–AS6 complex (cyan) and PYR1–ABA complex (gray, PDB code 3K90) at the ligand binding pocket. (**c**,**d**) Superposition of the PYR1–AS6 complex and the PYR1–ABA–HAB1 (orange, PDB code 3QN1) complex. The gate loop of the PYR1–AS6 complex adopted a closed conformation, and the AS6 *S*-hexyl chain passed through the 3′ tunnel to protrude over the PYR1 surface. In **c**, Val163 in the a3 helix and Val83 at the N terminus of the gate loop region are located at the top and bottom of the tunnel, respectively, and are highlighted in spheres. In **d**, the *S*-hexyl chain tip collided with HAB1 Val393, which is well conserved among PP2Cs (**d**).